ISBN: 978-3-95450-261-5 ISSN: 2673-7000 doi: 10.18429/JACoW-NAPAC2025-WEP042

HEAVY ION IMPLANTATION ANALYSIS IN GRAPHITE FOR THE FRIB CHARGE SELECTOR*

X. Wang †, T. Kanemura, A.S. Plastun, Facility for Rare Isotope Beams, East Lansing, MI, USA

Abstract

An advanced charge selector is currently under development at the Facility for Rare Isotope Beams (FRIB) to intercept unwanted charge states of stripped heavy ion beams. Rotating graphite wheels are employed to absorb beams with a power up to 5 kW and rms size as small as 0.7 mm × 1.25 mm.

Ion implantation and radiation damage can degrade material properties and lead to structural failure, making foreign ion accumulation a key factor in predicting graphite wheel lifetime. In this study, SRIM simulations and Monte Carlo analysis were used to model implantation with wheel geometry and rotation, followed by diffusion modeling. Results show that optimizing beam position and accounting for diffusion significantly reduce peak ion concentrations, providing essential data for graphite wheel lifetime assessment.

INTRODUCTION

The Facility for Rare Isotope Beams (FRIB), supported by the U.S. Department of Energy's Office of Science, is a state-of-the-art user facility dedicated to advancing nuclear science. Since commencing operations in 2022, FRIB has progressively increased its primary beam power from 1 kW to 20 kW [1]. The facility is now being upgraded for 50 kW operation, with the charge selector among the key devices under development [2].

The charge selector, located in the first folding segment of the accelerator, intercepts unwanted charge states produced after the beam stripper. An advanced design employing a rotating graphite wheel, shown in Fig. 1, is under development [3,4] to replace the existing unit . The upgraded system is designed to intercept beam spots with powers up to 5 kW, beam energies from 17 to 20 MeV/u, and rms sizes as small as 0.7 mm × 1.25 mm.

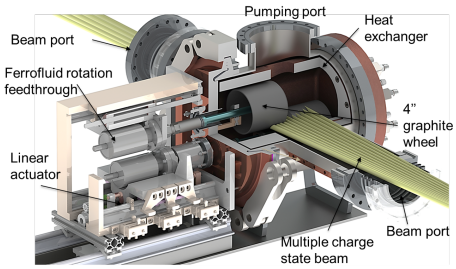

Figure 1: Model the charge selector.

* This material is based upon work supported by the U.S. Department of Energy, Office of Science, Office of Nuclear Physics and used resources of the Facility for Rare Isotope Beams (FRIB) Operations, which is a DOE Office of Science User Facility under Award Number DE-SC0023633.
† wangxiu@frib.msu.edu

As ion beams are continuously implanted into graphite, foreign ions, lattice displacement, and radiation damage accumulate in the material, potentially leading to structural failure [5, 6]. Therefore, determining the foreign ion accumulation behavior is one critical aspect for predicting the operational lifetime of graphite wheels.

After penetrating the graphite, the particles first come to rest through interactions with the target lattice [6]. Under the elevated operating temperatures of the graphite, these implanted particles then diffuse through the material, driven by concentration gradients [7, 8]. Once they diffuse to the surface, the foreign atoms evaporate into the surrounding vacuum environment [7, 9]. This study modeled the implantation and diffusion processes to support lifetime estimation.

METHODOLOGY

Ion Implantation and Rotation

As ions penetrate graphite, they lose energy through scattering events involving Coulomb interactions with the target's atoms and electrons, eventually coming to rest within the material. In this study, SRIM was used to simulate the scattering and stopping locations of ions in graphite. The resulting projected range distribution is described by Eq. (1).

$$\delta_{\text{depth}} = \frac{1}{\sqrt{2\pi}\,\sigma_{\text{depth}}} \exp\left(-\frac{(y-\mu_{\text{depth}})^2}{\sigma_{\text{depth}}^2}\right) \qquad (1)$$

where δ_{depth} is the projected range distribution, μ_{depth} and σ_{depth} are the mean stopping range and the projected straggling range, respectively.

To calculate the ion distribution in the graphite, a Monte Carlo–based model was developed to account for wheel geometry and rotational dynamics. Figure 2 shows the coordinates and calculation schematic: the beam strikes the wheel with the beam center at $(R - y_{\text{offset}}, z_0)$, where R is the wheel radius. The schematic shows a side view of the graphite wheel and illustrates the three main calculation steps.

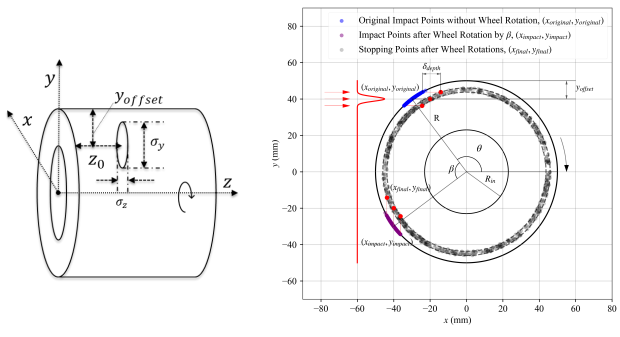

Figure 2: Coordinates (left); calculation schematic (right).

ISBN: 978-3-95450-261-5 ISSN: 2673-7000 doi: 10.18429/JACoW-NAPAC2025-WEP042

The simulation procedure begins by generating initial impact points based on the distribution of the beam, as shown in Eq. (2) and (3). The original points are shown as blue markers in the right plot of Fig. 2.

$$y_{\text{original}} = \frac{1}{\sqrt{2\pi}\sigma_y}\exp\left(-\frac{(y-y_0)^2}{2\sigma_y^2}\right) \quad -R < y_{\text{original}} < R \tag{2}$$

$$x_{\text{original}} = -\sqrt{R^2 - y_{\text{original}}^2} \quad , \theta = \arctan\left(\frac{y_{\text{original}}}{x_{\text{original}}}\right) \tag{3}$$

Subsequently, as the cylinder rotates by an angle β, the beam will impact new points on the graphite, with its coordinates calculated using Eq. (4). The new impact points are shown as purple markers in the right plot of Fig. 2.

$$x_{\text{impact}} = R \times \cos(\beta + \theta), \quad y_{\text{impact}} = R \times \sin(\beta + \theta) \tag{4}$$

The final ion coordinates can be determined using Eq. (5) and (6) by accounting for the penetration depth calculated by SRIM, as shown in Eq. (1). The final positions, shown as grey points in Fig. 2, are obtained after accounting for rotation.

$$x_{\text{final}} = x_{\text{impact}} + \delta_{\text{depth}} \times \cos(\beta) \tag{5}$$

$$y_{\text{final}} = y_{\text{impact}} + \delta_{\text{depth}} \times \sin(\beta) \tag{6}$$

Diffusion

After stopped in the graphite, the particles undergo diffusion driven by the concentration gradient. Owing to continuous irradiation, the graphite is maintained at an elevated temperature of approximately 1600 °C, which significantly enhances the diffusion rate in accordance with Arrhenius-type temperature dependence [10]. The diffusion process can be characterized by Fick's second law [10, 11], as expressed in Eq. (7).

$$\frac{\partial C}{\partial t} + D_A\left[\frac{1}{r}\frac{\partial}{\partial r}\left(r\frac{\partial C}{\partial r}\right) + \frac{\partial^2 C}{\partial z^2} + \frac{1}{r^2}\frac{\partial^2 C}{\partial \theta^2}\right] + \dot{S}(r,\theta,z) = 0 \tag{7}$$

where the C is volumetric concentration of foreign atoms, D_A is the diffusion coefficient, $\dot{S}(r,\theta,z)$ is the source term, representing the incoming ion rate and its spatial distribution.

The penetration depth of heavy ions is relatively short – typically a few hundred micrometers. Through diffusion, implanted ions can migrate to the graphite surface and subsequently escape into the surrounding vacuum. The fundamental physics of evaporation has been systematically studied by Hertz, Knudsen, and Langmuir. Based on their work, the surface evaporation rate can be calculated using Eq. (8), commonly referred to as the Hertz–Knudsen equation [12].

$$j_{\text{eva,max}} = \eta\left(P_v\sqrt{\frac{M}{2\pi RT}} - P\sqrt{\frac{M}{2\pi RT_g}}\right) \tag{8}$$

where M is the atomic weight, P_v is the saturation pressure, P is the pressure of the gas phase in the chamber, R is the universal gas constant, T and T_g are the temperatures of the foreign atoms and the bulk, respectively, and η is the evaporation coefficient, which has been reported equals to 1.66 in several studies [13, 14]. Evaporation defines the following boundary conditions for Eq. (7).

$$C = 0, \text{if } \frac{\partial}{\partial t}\left(\frac{\partial C}{\partial n}\right) \le j_{\text{eva,max}}, \tag{9}$$

$$\frac{\partial}{\partial t}\left(\frac{\partial C}{\partial n}\right) = j_{\text{eva,max}}, \text{if } \frac{\partial}{\partial t}\left(\frac{\partial C}{\partial n}\right) > j_{\text{eva,max}} \tag{10}$$

Calculation Parameters

In this work, we simulated ^{238}U implantation. The saturation pressure of uranium has been reported to range from 10^{-3} to 2×10^{-2} Pa at 1600 °C [15–17]. With the bulk temperature assumed to be at room temperature, and a vacuum of 10^{-7} mbar [4], $j_{\text{eva,max}}$ is calculated to range from 6.39×10^{12} to 1.3×10^{14} atoms/mm^2/s. Tallent et al. [18] and Loch et al. [19] measured the diffusion coefficient of ^{238}U in graphite at elevated temperatures. Using the Arrhenius equation [10] to interpolate between their measurements, the diffusion coefficient of ^{238}U through graphite at 1600 °C is estimated to range from 10^{-12} to 10^{-10} cm^2/s.

RESULTS AND DISCUSSION

Ion Distribution with Rotation

After obtaining the final coordinates of the incident particles in the Monte Carlo–based analytical model, a statistical analysis was performed, which revealed that the foreign ion concentration can be fitted using Eq. (11).

$$\rho(r) = \frac{1}{\sqrt{2\pi}\,\sigma_{\text{fit}}}\exp\left(-\frac{(r-r_{0,\text{fit}})^2}{2\sigma_{\text{fit}}^2}\right) \tag{11}$$

where $\rho(r)$ is the normalized density along the r direction, σ_{fit} is the standard deviation, $r_{0,\text{fit}}$ is the mean radial position. In SRIM, the mean stopping range and projected straggling range are 186 μm and 0.7 μm, respectively; in the rotating-wheel scenario, the fitted mean position μ_{fit} and deviation σ_r are 49.888 mm (112 μm from the surface) and 6.2 μm, respectively. These results show that wheel rotation reduces the peak concentration by about 10 times and shifts the mean depth by about 74 μm toward the surface, shortening the diffusion path to the surface.

As a result, combining the deviations in the z- and r-direction with angular variation, the implanted ion distribution with rotation can be expressed by Eq. (12).

$$\dot{S}(r,\theta,z) = \frac{I}{2\pi\sigma_r\sigma_z}\cdot\frac{1}{2\pi r} \times \exp\left(-\frac{(r-r_0)^2}{2\sigma_r^2}\right)\exp\left(-\frac{(z-z_0)^2}{2\sigma_z^2}\right) \tag{12}$$

Ion Distribution with Diffusion

The diffusion process is solved using the finite volume method with implicit Euler time integration for two diffusion

ISBN: 978-3-95450-261-5 ISSN: 2673-7000 doi: 10.18429/JACoW-NAPAC2025-WEP042

coefficients. For each diffusion coefficient, sixteen simulation cases were conducted, with mesh resolution varied over two times and time step over three times. Mesh and time-step independence are verified by evaluating peak concentration deviations against the ultra-small (XS) mesh/time-step case, with all deviations below 0.25 %, as shown in Table 1.

Table 1: Relative Deviation of the Peak Concentration at Day 30 for Various Mesh Resolutions and Time Steps Δt

Δt	Mesh resolution			
	Coarse	**Moderate**	**Fine**	**XS**
Coarse	0.14 %	0.15 %	0.21 %	0.21 %
Moderate	0.08 %	0.08 %	0.12 %	0.12 %
Small	0.01 %	0.01 %	0.03 %	0.03 %
XS	-0.02 %	-0.01%	0.00 %	N/A

Figures 3 and 4 show the concentration profile and its projection for a diffusion coefficient of 10^{-10} cm^2/s after 30 days of implantation and diffusion. The results shows a clear concentration gradient in the *r*-*z* plane with the peak concentration near the source and gradually decreasing with distance. Besides, the particle spread is several times the source width in *r* but remains comparable in *z*, reflecting the steeper *r*-direction concentration gradient.

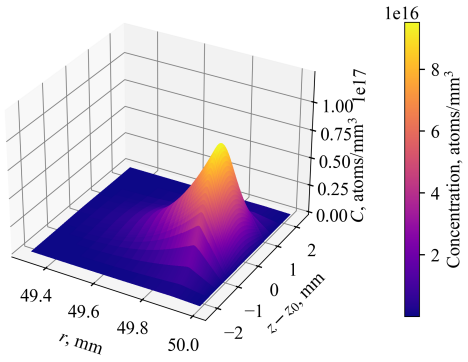

Figure 3: Ion distribution in the *r*-*z* plane.

Figure 5 presents the maximum concentration and the surface evaporation rate over a 60-day period with ^{238}U implantation occurring during the first 30 days. Following ^{238}U implantation, continued irradiation keeps the graphite at an elevated temperature; therefore, the diffusion coefficient is assumed constant.

The highest peak concentration for 10^{-10} cm^2/s reaches 10^{17} atoms/mm^3, which is ten times lower than that for 10^{-12} cm^2/s. With a graphite atomic density of 9.03 × 10^{19} atoms/mm^3, the corresponding atomic implantation ratio ranges from 0.11% to 1.1%. At $D_A = 1 \times 10^{-10}$ cm^2/s, the peak concentration is 10 times lower than without diffusion. After ^{238}U implantation ceases, its concentration decreases due to diffusion. During the process, higher diffusion coefficients result in an increased evaporation rate, while the evaporation rate remains significantly below the maximum theoretical limit $j_{\mathrm{eva,max}}$.

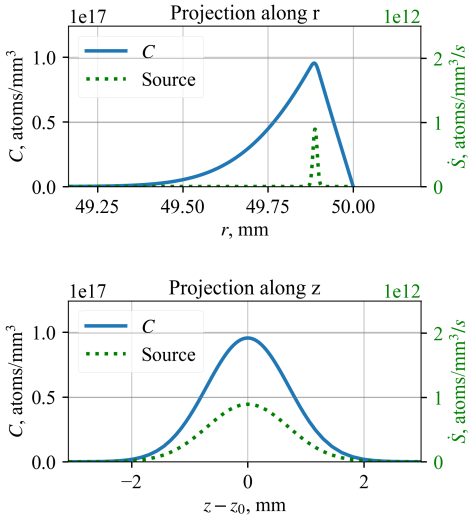

Figure 4: Projection of the concentration.

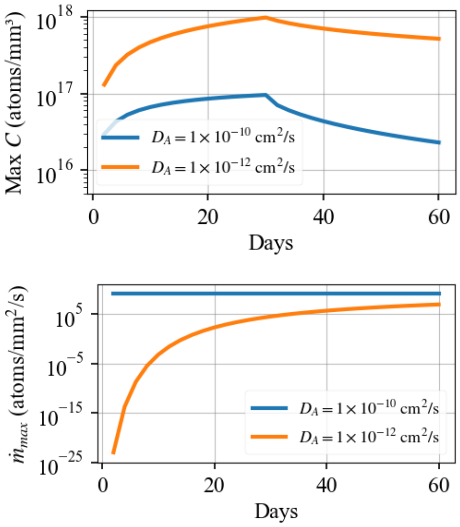

Figure 5: Evolution of the maximum concentration (top) and the maximum evaporation rate at the surface (bottom) over a 60-day period, with first 30 days of ^{238}U implantation.

CONCLUSION

Heavy ion implantation in graphite was systematically modeled, incorporating the effects of rotation, geometry, diffusion, and surface release. Using ^{238}U as the implanted species, the analysis shows that geometry and rotation reduce the peak concentration by about 10 times. After 30 days of implantation, the peak concentration is 1×10^{18} atoms/mm^3 (1.1% of the graphite atomic density) for 1×10^{-12} cm^2/s and 1×10^{17} atoms/mm^3 (0.11%) for 1×10^{-10} cm^2/s, both indicating substantial retention. These results quantify the implantation behavior in the FRIB advanced charge selector and offer critical insights for graphite lifetime estimation.

REFERENCES

[1] J. Wei *et al.*, "FRIB operations: First three years", in *Proc. HIAT2025*, Michigan State University, East Lansing, USA,

ISBN: 978-3-95450-261-5 ISSN: 2673-7000 doi: 10.18429/JACoW-NAPAC2025-WEP042

Jun. 2025, paper MOX01, to be published.

[2] T. Kanemura *et al.*, "High power targetry devices at frib: Challenges, status and plan", in *Proc. HIAT2025*, Michigan State University, East Lansing, USA, Jun. 2025, paper MOZ03, to be published.

[3] A. Plastun *et al.*, "Advanced charge selector for stripped heavy ion beams", in *Proc. IPAC'24*, Nashville, TN, USA, May 2024, pp. 1582–1585, 2024. doi:10.18429/JACoW-IPAC2024-TUPR70

[4] X. Wang *et al.*, "Monte-carlo simulation of vacuum system for advanced charge selector", in *Proc. HIAT2025*, Michigan State University, East Lansing, USA, Jun. 2025, paper TUP06, to be published.

[5] B. S. Elman, M. Hom, E. W. Maby, and M. S. Dresselhaus, "Ion-implantation studies of graphite", *MRS Online Proceedings Library (OPL)*, vol. 20, p. 341, 1982. doi:10.1557/PROC-20-341

[6] M. S. Dresselhaus and R. Kalish, *Ion Implantation in Diamond, Graphite and Related Materials*. Springer Berlin Heidelberg, 1992, vol. 22. doi:10.1007/978-3-642-77171-2

[7] A. Chakrabarti, V. Naik, and S. Dechoudhury, *Rare Isotope Beams: Concepts and Techniques*. CRC Press, 2021. doi:10.1201/9780429185885

[8] G. J. Beyer, E. Hagebø, A. F. Novgorodov, and H. L. Ravn, "The role of diffusion in ISOL targets for the production of radioactive ion beams", *Nucl. Instrum. Methods Phys. Res., Sect. B*, vol. 204, pp. 225–234, 2003. doi:10.1016/S0168-583X(02)01913-4

[9] R. W. Balluffi, S. M. Allen, and W. C. Carter, *Kinetics of materials*, R. A. Kemper, Ed. Wiley-Interscience, 2005. doi:10.1002/0471749311

[10] H. Mehrer, *Diffusion in solid*. Springer Berlin, Heidelberg, 2007. doi:10.1007/978-3-540-71488-0

[11] J. Crank, *The mathematics of diffusion*, 2. ed., reprint. Clarendon Press, 1976.

[12] M. A. Herman, W. Richter, and H. Sitter, *Epitaxy: Physical Principles and Technical Implementation*. Springer Science & Business Media, 2013.

[13] "Vacuum evaporation of pure metals", *Metall Mater Trans A*, vol. 44, no. 2, pp. 747–753, 2013. doi:10.1007/s11661-012-1464-2

[14] T. Kanemura, H. Kondo, T. Furukawa, Y. Hirakawa, E. Wakai, and J. Knaster, "Analytical and experimental study of the evaporation and deposition rates from a high-speed liquid lithium jet", *Fusion Eng. Des.*, vol. 122, pp. 176–185, 2017. doi:10.1016/j.fusengdes.2017.08.020

[15] E. G. Rauh and R. J. Thron, "Vapor pressure of uranium", Chemistry-General, 1954. https://www.osti.gov/servlets/purl/4402017

[16] C. B. Alcock, V. P. Itkin, and M. K. Horrigan, "Vapour pressure equations for the metallic elements: 298–2500k", *Can. Metall. Q.*, vol. 23, pp. 309–313. doi:10.1179/cmq.1984.23.3.309

[17] V. Venugopal, S. G. Kulkarni, C. S. Subbanna, and D. D. Sood, "Vapour pressures of uranium and uranium nitride over UN(s)", *J. Nucl. Mater.*, vol. 186, no. 3, pp. 259–268, 1992. doi:10.1016/0022-3115(92)90345-L

[18] O. K. Tallent, R. P. Wichner, L. Roy, and H. Towns, "Uranium diffusion in h-451 graphite", *Nucl. Technol.*, vol. 68, no. 3, pp. 336–343, 1985. doi:10.13182/NT85-A33579

[19] L. D. Loch, J. R. Gambino, and W. H. Duckworth, "Diffusion of uranium through graphite", *AIChE Journal*, vol. 2, no. 2, pp. 195–198, 1956. doi:10.1002/aic.690020213